Astron. Astrophys. Suppl. Ser. 118, 329-380 (1996)

The MOST supernova remnant catalogue (MSC)

J.B.Z. Whiteoak^{1,2} and A.J. Green²

- ¹ Max-Planck-Institut für Radioastronomie, Auf dem Hügel 69, 53121 Bonn, Germany
- ² School of Physics, University of Sydney, Sydney N.S.W. 2006, Australia

Received June 2; accepted August 19, 1995

Abstract. — A catalogue of supernova remnants in the southern Galaxy within the area $245^{\circ} \le l \le 355^{\circ}$, $|b| \lesssim 1.5^{\circ}$ has been produced from observations made at 0.843 GHz with a resolution of 43" using the Molonglo Observatory Synthesis Telescope (MOST). The catalogue, presented here, provides greyscale images and contour maps of known and newly-discovered remnants. The increased resolution and sensitivity of these observations has resulted in better statistics for southern remnants.

Key words: ISM: supernova remnants — radio continuum: ISM — atlases — catalogues — surveys

1. Introduction

Supernovae represent a cataclysmic event in the evolution of massive stars in which expelled material and associated shocks move outward and interact with and violently restructure the interstellar medium (ISM). Although no supernovae have been observed in our Galaxy since radio astronomy began, numerous past explosions have left their fingerprints on the ISM as supernova remnants (SNRs). Because of their steep spectral index, low-frequency radio observations are particularly appropriate for the study of SNRs. The Molonglo Observatory Synthesis Telescope (MOST), operating in the continuum at 0.843 GHz, is very well suited because of its sensitivity to low-brightness structure. In addition, its higher resolution ($\sim 43''$) has allowed the detailed structure of many objects to be viewed for the first time.

At present, observations of 182 SNRs have been published in D.A. Green's (1995) all-sky catalogue. A recently-completed survey of the southern Galactic plane using the MOST has been systematically inspected for new information concerning both previously-known and newly-discovered SNRs. Identification of new SNRs is made on the basis of a characteristic shell structure. The high-frequency radio continuum surveys currently available are confusion-limited near large, complex thermal regions where SNRs are often located, and so it is difficult to confirm in many cases whether these new SNR candidates have non-thermal spectral indices. Data from the IRAS survey offer a more promising alternative. Thermal and non-thermal sources differ significantly in their ratio of

 $60~\mu m$ to radio flux densities (e.g. Broadbent et al. 1989), and this allows the reliable identification of many objects. However, this method may be inconclusive for faint radio objects, and at present several of the suggested candidates cannot be confirmed. Polarisation measurements have also been conducted for a small number of objects using the Parkes radio telescope.

The MOST Galactic plane survey covers the region $245^{\circ} \leq l \leq 355^{\circ}$, $|b| \leq 1.5^{\circ}$ in a series of 650 overlapping fields. Green's (1995) catalogue of SNRs lists 55 objects which are wholly or partly observed in the MOST survey. Greyscale and contour maps have been prepared for these sources, forming the first part of the MOST supernova remnant catalogue (MSC.A). About 40% of these SNRs have previously been observed with the MOST, but only a limited number have been published with the sensitivity and fidelity now available. Two objects from the 55 have been resolved into unrelated components and rejected as SNRs. In addition, four objects which were originally published as SNRs and subsequently rejected by Green (1995) from the limited data available previously, have now been re-confirmed as remnants.

The second part of the catalogue, MSC.B, presents 18 new SNRs discovered in the MOST survey, identified both through their characteristic shell structure and because they satisfy the $60~\mu\mathrm{m}/\mathrm{radio}$ flux density criterion. All the fields in the survey were inspected for possible remnants. However, shell structure is only detectable in remnants whose diameters are $\gtrsim 4'$ which is the limit set by the telescope resolution. Part three of the catalogue, MSC.C, contains 16 sources that are possible SNRs. While many

of these have typical shell structure, they are very faint and their identification as SNRs is only tentative.

2. Observations

The observations are part of a recently completed survey of the southern Galactic plane at 0.843 GHz using the MOST (Mills 1981; Robertson 1991) that covers the region $245^{\circ} \leq l \leq 355^{\circ}$, $|b| \leq 1.5^{\circ}$ (Whiteoak et al. 1989). Each of the 650 fields in the survey covers an area of $70' \times 70'$ cosec(δ) (R.A. × Dec.), and was observed over a 12 hr period. The resolution achieved is $43'' \times 43''$ cosec(δ) and the sensitivity ~ 2 mJy/beam.

Four calibration sources were observed immediately before and after each 12 hr observation to establish pointing and flux density calibration. Positional uncertainty is $\sim 1''$. The flux density scale is based on the reference source 1934–638 for which $S_{0.843}=13.65$ Jy. For unresolved sources stronger than about 20 mJy, the flux density uncertainty is $\sim 7\%$. For extended SNRs, baselevel uncertainties result in integrated flux densities with errors $\sim 10\%$, increasing to 30% for very faint objects. The MOST does not measure visibilities on baselines $\lesssim 15$ m and so is not sensitive to smooth structure on a scale $\gtrsim 30'$. For SNRs with large angular diameter, the flux density may then be underestimated, and hence only a lower limit is given.

Several of the maps presented contain telescope artifacts. The most obvious are grating rings which appear as narrow, faint rings of radius 1.2°. Another artifact appears as faint rays originating from bright sources, a result of atmospheric fluctuations and calibration errors. Bright extended sources are surrounded by regions of apparently negative emission caused by the absence of low spatial frequencies in the data.

Many of the images presented in this paper are mosaics of two or more individual fields, and the sensitivity is thus often better than 2 mJy/beam. Most of the fields have been CLEANed using the AIPS task APCLN, while several have been deconvolved using the maximum entropy algorithm VTESS. In general, all components down to a level of ~ 7 mJy/beam were removed during CLEANing, although the limit depended on the object and was generally lower for faint SNRs.

3. Results

In the investigation of SNRs in the MOST survey, it was important to establish systematic criteria for the identification of possible remnants. Objects already known were studied for improved information and in some cases a reassessment of their classification. The preliminary images of the entire MOST survey were then inspected for possible new identifications, although the presence of telescope artifacts may still have masked some candidates. The completeness of the search is discussed in the next section.

A characteristic shell structure was the primary criterion in the identification of new remnants. It is possible to detect recognisable structure in sources with diameters $\gtrsim 4'$. It is also possible to detect parts of large-diameter SNR shells if small-scale gradients exist in their surface brightness. Establishing whether a shell was non-thermal was sometimes difficult, particularly if it was faint. The high-frequency radio continuum surveys currently available are often lacking in either the sensitivity or the resolution required for accurate spectral index measurements.

The ratio of 60 μ m to 0.843 GHz flux densities has been a useful indicator in discriminating between thermal and non-thermal radio emission, especially for small-diameter sources (Whiteoak 1992). Typical flux density ratios for commonly-encountered objects are given in Table 1. Supernova remnants generally have very low flux density ratios and can be reliably identified on this basis. However, this method was inconclusive for several weak extended sources because of confusion with faint 60 μ m emission associated with such phases of the medium as H II . These sources have been listed in MSC.C, including several small-diameter candidates which are non-thermal but at this stage not precisely identified. Higher-resolution studies are planned for these sources.

The three parts of the catalogue are presented as Tables MSC.A, MSC.B and MSC.C. In each Table, Col. 1 gives the Galactic name of the remnant. In MSC.A, this is generally the name as previously published. Column 2 gives the position of the geometric centre of the SNR in J2000.0 coordinates. When the object does not have a complete shell, the centre and dimensions of the ring which best describes the remnant are used. The integrated flux density $S_{0.843}$ is given in Col. 3, which may be a lower limit for large objects. Column 4 is the angular size, $\Theta_{0.843}$, giving the major and minor diameters of the shell or the equivalent elliptical ring as described for Col. 2. Column 5 lists the mean surface brightness, $\Sigma_{0.843}$. The type of SNR is described in Col. 6 as shell (S), plerion or filledcentre (P), or composite (C). An asterisk after the SNR type indicates apparent multiple shell structure. The SNR type differs from Green's (1995) classification in 25\% of the sources common to both catalogues, reflecting the improved sensitivity and resolution of the MOST images. The Figure number is given in Col. 7. Columns 8 and 9 apply only to MSC.A and give, respectively, the references to previous MOST publications and common names by which the remnants are known. The final column in MSC.C gives a brief description of each object. Following the text, Figs. 1-35 show greyscale images and contour maps for SNRs listed in MSC.A and MSC.B. Contour levels are indicated below each map, with negative contours shown dotted. In several maps the lowest positive contour is also dotted to emphasise structure more clearly. The two objects which are no longer classified as SNRs are shown in Fig. 36.

Class of Object	R
Compact H II regions	≥1000
Extended HII regions	$\gtrsim 500$
Planetary nebulae (optically thick)	$\gtrsim 400$
Planetary nebulae (optically thin)	50 - 400
Extragalactic objects (gas-rich spirals)	50 - 200
Extragalactic objects (others)	~ 0
SNRs	$\lesssim 50$

Table 1. Typical values of the ratio R of 60 μ m to 0.843 GHz flux densities for various objects

Notes on selected SNRs from MSC.A and MSC.B are now given.

3.1. MSC.A Sources

G263.9-3.3: (Fig. 1) The MOST image shows a small section of the shell of the Vela SNR. The emission sweeps across the field in curtains of low-brightness, parallel filaments (Whiteoak et al. 1989). In the north-western quarter of this particular field, the filaments converge and curve to the west, and they are generally found to lie orthogonally to the direction of the centre of Vela (situated 3° away to the south-west). Comparison with the optical emission in SERC-J plates shows that there is often a spatial correspondence between the radio and optical filaments, although the brightest of the radio filaments have no optical counterparts and vice versa. A similar phenomenon has been noted by van den Bergh et al. (1973). The emission in the field shown is typical of the structure found in many other fields near Vela observed with the MOST, and shows for the first time the filamentary nature of the radio emission associated with this remnant.

G279.0+1.1: (Fig. 1) A large-diameter shell SNR of low brightness discovered by Woermann & Jonas (1988), only partially lying within the MOST survey. The image shows that at least part of the emission attributed to the shell in their observations comes from a bright, unresolved non-thermal source at R.A. (J2000) = $9^{\rm h}52^{\rm m}38.5^{\rm s}$, Dec. (J2000) = $-53^{\circ}15'06''$ which is probably an extragalactic object. The structure resembles the shell emission from the Vela SNR, with faint filaments extending over several degrees.

G290.1—0.8: (Fig. 2) This source does not possess the well-defined annular brightness distribution common to shell SNRs, but shows considerable complex internal structure. The overall shape is elongated, with weak lobes at both ends of the longer axis, suggesting 'blowouts' in opposition. The brightest radio emission occurs on the south-western edge (Milne et al. 1989), coinciding with prominent optical filaments that are superposed on a more diffuse component found to be roughly coextensive with

the radio source (Elliott & Malin 1979). X-rays coincide with the radio emission and show enhancements in the two lobe regions (Seward 1990). Unlike the radio emission, however, the X-rays are strongly peaked towards the remnant centre.

G291.0-0.1: (Fig. 2) This SNR has an unusual composite morphology that resembles a trident, with three roughly parallel ridges aligned at $P.A.=45^{\circ}$ lying within a circular region of fainter emission. The two outer ridges may be part of a shell structure while the brighter central ridge may be a plerionic component. Roger et al. (1986) favour a filled-centre interpretation for the overall emission and suggest that the outer ridges are merely subsidiary peaks. Plerionic X-ray emission has been detected from the remnant (Wilson 1986; Seward 1990), consisting of a bright core of diameter 2' lying within faint emission that roughly matches the radio region. The peak of the X-ray emission is displaced 1.7' to the south-west of the radio peak along the central radio ridge (Roger et al. 1986; Wilson 1986). The elongation of the X-ray core coincides with the longer axis of the radio ridge, and its brightness drops sharply on its south-western edge, but more gradually on its north-eastern edge, suggesting proper motion of an object in a south-westerly direction along the ridge. Wilson (1986) finds a narrow ridge of X-ray emission extending northwards from the western side of the SNR with signs that it could extend as far as 16' from the core. There is evidence of a faint radio counterpart of this ridge in the MOST image.

G293.8+0.6: (Fig. 3) A composite SNR. The shell component is circular and faint, while the plerionic component consists of a region of relatively bright emission at the shell centre. The shell and plerionic components contribute respectively 2.1 and 0.5 Jy to the total flux density.

G296.1-0.5: (Fig. 3) This SNR has an unusual structure consisting of four disconnected filamentary bands of emission defining an irregular shell. There is essentially no emission along the north-eastern border, and little emission from within the shell. The MOST image presented here suggests that all of the non-thermal radio emission

Table MSC.A. Parameters of known SNRs

Name	Position (J2000.0)	S	Θ	Σ	Type	Fig.	MOST	Common
Ivallie	R.A. Dec.	$S_{0.843}$	$\Theta_{0.843}$	$\Sigma_{0.843} \ (\times 10^{-21})$	туре	No.	Ref.	Name
	(h m s, °')	(Jy)	('×')	$(Wm^{-2}Hz^{-1}sr^{-1})$		110.	rter.	rame
(1)	(2)	(3)	(4)	(Will 112 Si) (5)	(6)	(7)	(8)	(9)
G263.9 - 3.3	08 44 00, -43 40				\mathbf{C}	1	13	Vela(X,Y,Z)
G279.0+1.1	09 57 00, -53 50		10 14		S	1		MCII 11 044
G290.1-0.8	11 03 00, -60 54	43	19×14	30	S	2	5,10	MSH 11-6 <i>1</i> A
G291.0-0.1	11 12 00, -60 38	12.7	15×13	7.5	C? C	2	12 5	
G293.8+0.6 G296.1-0.5	$11 \ 35 \ 00, -60 \ 54$ $11 \ 51 \ 00, -62 \ 34$	2.6 > 2.4	$\begin{array}{c} 21 \times 19 \\ 37 \times 25 \end{array}$	1.0 > 0.4	s	3 3		
G296.1=0.3 G296.8=0.3	$11\ 51\ 00,\ -62\ 34$ $11\ 58\ 30,\ -62\ 35$	9.2	20×14	5.4	S*	4		1156-62
G298.5 - 0.3	$12\ 12\ 30,\ -62\ 54$	1.8	07×02	15	?	4		1100-02
G298.6-0.0	$12\ 13\ 30,\ -62\ 37$	7.4	12×09	10	S	5	5	
G302.3+0.7	12 46 00, -62 09	3.2	18×16	1.7	s*	5		
G304.6+0.1	$13\ 05\ 50,\ -62\ 42$	18	08×08	40	S	6		Kes 17
G308.7 + 0.0	$13\ 41\ 30,\ -62\ 15$	9.9	22×08	8.8	S?	6	3	
G309.2 - 0.6	$13\ 46\ 40,\ -62\ 54$	6.0	15×12	5.4	S^*	7	5	
G309.8+0.0	$13\ 50\ 30,\ -62\ 04$	>8.8	25×19	>2.8	S	7		
G310.6 - 0.3	$13\ 58\ 00,\ -62\ 09$	5.4	09×08	11	\mathbf{S}	8		Kes 20B
G310.8 - 0.4	$14\ 00\ 00,\ -62\ 17$	6.9	12×12	7.0	\mathbf{S}	8		Kes 20A
G311.5 - 0.3	$14\ 05\ 35,\ -61\ 54$	2.9	05×04	19	S	8		
G312.4 - 0.4	$14\ 13\ 20,\ -61\ 48$	>19	38×37	>2.6	S	9		
G315.4-0.3	14 35 40, -60 36	3.1	24×13	1.4	?	9		DOWN ON MOULT A GO ON 105
G315.4-2.3	$14\ 42\ 30,\ -62\ 27$	>22	43×40	>1.8	S*	10	5,8	RCW 86, MSH 14-63, SN 185
G315.9-0.0	14 38 30, -60 11	$\frac{0.9}{20}$	25×14	0.5	S S*	10	6	
G316.3-0.0	$14\ 41\ 20,\ -60\ 03$ $14\ 58\ 20,\ -58\ 28$	4.8	29×14 30×14	$6.6 \\ 2.1$	C*	11 11	5,8,9 $14,16$	
G318.9+0.4 G320.4-1.2	14 56 20, -56 26 15 14 20, -59 11	62	36×33	9.6	S?	$\frac{11}{12}$	7	RCW 89, MSH 15-52
G320.4-1.2 G320.6-1.6	15 17 50, -59 16	>9.3	60×30	>0.7	S*	12		100 W 89, WISH 13-52
G321.9-0.3	15 20 40, -57 36	>8.3	31×23	>1.8	S	13	4,5	
G322.5-0.1	$15\ 23\ 20,\ -57\ 06$	1.7	16×14	1.2	$\tilde{\mathbf{c}}$	13	15	
G323.5+0.1	$15\ 28\ 50,\ -56\ 23$	4.2	13×12	4.9	S	14		
G326.3 - 1.8	$15\ 53\ 00,\ -56\ 09$	> 130	40×36	>14	$^{\rm C}$	14	5,8,10	MSH 15-56
G327.1 - 1.1	$15\ 54\ 20,\ -55\ 06$	7.6	19×17	3.5	$^{\rm C}$	15		
G327.4+0.4	$15\ 48\ 20,\ -53\ 46$	25	23×19	8.5	S^*	15	5,8,10	Kes 27
G328.4+0.2	$15\ 55\ 30,\ -53\ 17$	15	06×06	60	\mathbf{C} ?	16		
G330.2+1.0	$16\ 01\ 00,\ -51\ 34$	4.7	12×10	6.0	C?	16	1	
G332.0+0.2	$16\ 13\ 10,\ -50\ 57$	8.9	12×12	10	S	17	5	
G332.4+0.1	$16\ 15\ 10,\ -50\ 42$	29	17×13	20	S*	17	6,8,9,11	Kes 32, MSH 16-51
G332.4-0.4	16 17 40, -51 03	34	11×10	52	S	18	5	RCW 103
G335.2+0.1	$16\ 27\ 30,\ -48\ 45$ $16\ 32\ 00,\ -47\ 19$	16	$\begin{array}{c} 22 \times 20 \\ 14 \times 10 \end{array}$	5.9	S S*	18		MSH 16-44
G336.7+0.5 G337.0-0.1	16 35 50, -47 37	$\frac{6.1}{21}$	14×10 13×07	$\frac{6.4}{42}$	S?	19 19	5,8	
G337.2-0.7	16 39 30, -47 50	2.0	06×06	11	S.	20		
G337.3+1.0	16 32 40, -46 36	20	15×12	22	S	20	5,8,10	Kes 40
G337.8-0.1	16 39 00, -46 58	18	09×06	48	Š	21		Kes 41
G338.1+0.4	$16\ 37\ 50,\ -46\ 26$	3.8	16×14	3.0	S	21		
G338.3 - 0.0	$16\ 40\ 50,\ -46\ 32$	7.4	09×08	15	S	22		
G338.5 + 0.1	16 41 00, -46 17	13	10×07	37	S	22		
G340.4+0.4	$16\ 46\ 30,\ -44\ 39$	5.9	10×07	17	S*	23		
G340.6+0.3	$16\ 47\ 40,\ -44\ 34$	4.5	07×06	22	S	23		
G341.9 - 0.3	$16\ 54\ 50,\ -44\ 01$	2.7	07×07	7.6	S*	23		
G342.0-0.2	$16\ 54\ 50,\ -43\ 53$	3.5	12×09	6.2	S	23		
G344.7-0.1	17 04 00, -41 43	2.5	10×10	4.2	S*	24		
G346.6-0.2	17 10 20, -40 12	8.7	11×10	18	S C*	24	• • •	CITID 27A
G348.5+0.1	17 14 40, -38 32	71	19×16	54	S*	25		CTB 37A
G348.5-0.0	$17\ 15\ 15,\ -38\ 31$ $17\ 14\ 10,\ -38\ 14$	10.2	09×08 18×16	19	S S*	$\frac{25}{25}$		CTB 37B
G348.7+0.3 G349.7+0.2	$17\ 14\ 10, -38\ 14$ $17\ 18\ 00, -37\ 27$	$\frac{33}{22}$	03×02	$18 \\ 170$	S?	$\frac{25}{25}$	• • • •	O1D 9/D
G349.7+0.2 G351.2+0.1	$17\ 18\ 00,\ -37\ 27$ $17\ 22\ 25,\ -36\ 11$	5.5	$03 \times 02 \\ 08 \times 07$	15	S:	26	2	
G352.7-0.1	17 27 40, -35 07	4.4	08×06	14	S*	26		
G552.1-0.1	11 21 40, -33 01	4.4	00 \ 00	1.4	b	20		

References: (1) Caswell et al. (1983b), (2) Caswell et al. (1983c), (3) Caswell et al. (1992), (4) Haynes (1987), (5) Kesteven & Caswell (1987), (6) Kesteven et al. (1987), (7) Manchester & Durdin (1983), (8) Milne et al. (1985), (9) Milne et al. (1988), (10) Milne et al. (1989), (11) Roger et al. (1985), (12) Roger et al. (1986), (13) Whiteoak et al. (1989), (14) Whiteoak (1990), (15) Whiteoak (1992), (16) Whiteoak (1993a).

Table MSC.B. Parameters of new SNRs

Name	Position (J2000.0)	$S_{0.843}$	$\Theta_{0.843}$	$\Sigma_{0.843}$	Type	Fig.
	R.A. Dec.			$(\times 10^{-21})$		No.
	(h m s, o')	(Jy)	$(' \times ')$	$(Wm^{-2}Hz^{-1}sr^{-1})$		
(1)	(2)	(3)	(4)	(5)	(6)	(7)
G286.5-1.2	10 35 40, -59 42	1.6	26×6		S?	27
G289.7 - 0.3	$11\ 01\ 10,\ -60\ 18$	6.4	18×8	3.3	S^*	27
G294.1 - 0.0	$11\ 36\ 10,\ -61\ 39$	> 2	40×40	> 0.2	S	28
G299.6 - 0.5	$12\ 21\ 50,\ -63\ 09$	1.1	13×13	0.9	S	28
G301.4 - 1.0	$12\ 38\ 00,\ -63\ 49$	2.3	37×23	0.5	S	29
G308.1 - 0.7	$13\ 37\ 40,\ -63\ 04$	1.3	16×14	0.9	S	29
G317.3 - 0.2	$14\ 49\ 40,\ -59\ 46$	5.2	12×10	5.6	S	30
G318.2+0.1	$14\ 54\ 50,\ -59\ 03$	> 4.3	40×35	> 0.4	S	30
G321.9 - 1.1	$15\ 23\ 50,\ -58\ 13$	> 3.8	28×28	> 0.6	S	31
G327.4 + 1.0	$15\ 46\ 50,\ -53\ 20$	2.1	14×13	2.0	S	31
G329.7 + 0.4	$16\ 01\ 20,\ -52\ 19$	> 38	40×33	> 4.3	S^*	32
G342.1+0.9	$16\ 50\ 40,\ -43\ 04$	0.6	10×9	1.0	S	32
G343.1 - 0.7	$17\ 00\ 20,\ -43\ 14$	8.5	27×21	2.6	S^*	33
G345.7 - 0.2	$17\ 07\ 20,\ -40\ 53$	0.7	07×05	2.8	S	33
G349.2 - 0.1	$17\ 17\ 20,\ -38\ 04$	1.6	09×06	5.0	S	34
G351.7 + 0.8	$17\ 21\ 00,\ -35\ 27$	11	18×14	6.4	S	34
G351.9 - 0.9	$17\ 28\ 50,\ -36\ 16$	2.0	12×09	2.8	S	35
G354.8 - 0.8	$17\ 36\ 00,\ -33\ 42$	3.1	20×18	1.4	S	35

Table MSC.C. Parameters of possible SNRs

Name	Position (J2000.0) R.A. Dec.	$S_{0.843}$	$\Theta_{0.843}$	$\Sigma_{0.843} \ (\times 10^{-21})$	Comment
(1)	(h m s, ° ') (2)	(Jy) (3)	$(^{\prime}\times^{\prime})$	$(Wm^{-2}Hz^{-1}sr^{-1})$ (5)	(6)
G308.4-1.4	13 41 25, -63 45 06	0.8	14×04	1.3	Several arcs
G317.5 + 0.9	$14\ 47\ 16,\ -58\ 36\ 33$	0.4	30×25	0.09	Faint incomplete shell
G319.9 - 0.7	$15\ 09\ 14,\ -58\ 54\ 26$	0.9	06×02	2.3	Linear structure with central bulge
G320.6 - 0.9	$15\ 15\ 03,\ -58\ 46\ 55$	0.5	03×03	5.8	Centrally-peaked disk
G322.7+0.1	15 23 56, -56 48 41	0.3	12×11	0.2	Very faint disk/shell
G322.9 - 0.0	15 25 41, -56 46 16	0.4	14×11	0.4	Very faint disk/shell
G323.2 - 1.0	$15\ 31\ 41,\ -57\ 23\ 55$	0.3	06×04	1.0	Amorphous structure within faint shell
G324.1+0.1	15 32 32, -56 03 08	1.2	14×06	1.8	Elongated shell
G325.0 - 0.3	15 39 13, -55 49 45	0.2	04×04	1.6	Faint shell
G331.8 - 0.0	16 13 13, -51 11 38	0.4	02×01	14	Elongated blob
G337.2+0.1	$16\ 35\ 57,\ -47\ 19\ 00$	1.4	03×02	23	Bright blob
G339.6 - 0.6	$16\ 48\ 04,\ -45\ 52\ 17$	0.7	03×02	11	Elongated blob
G345.1+0.2	17 03 40, -41 05 11	0.7	10×10	0.7	Faint shell
G345.1 - 0.2	$17\ 05\ 21,\ -41\ 26\ 04$	1.8	06×06	7.1	Bright shell with point source
G348.8 + 1.1	17 11 29, -37 35 39	0.1	10×10	0.1	Faint, incomplete shell
G350.1 - 0.3	$17\ 21\ 01,\ -37\ 25\ 57$	5.0	06×03	24	Elongated structure

in the region is part of a single SNR, a subject of much previous debate (e.g. Caswell & Barnes 1983). Bright X-ray emission is coincident with three of the four bands: the band defining the northern boundary and the two in the south-western quarter of the image (Markert et al. 1981; Bignami et al. 1986; Seward 1990). There is reasonable spatial correlation between the radio and X-ray emission, although the relative intensities of the different regions do not correlate well. Longmore et al. (1977) and Hutchings, Crampton & Cowley (1981) found faint optical nebulosity in the west around the northern part of the brightest radio band. The diffuse radio emission in the north-western corner of the MOST image is thermal and probably unrelated to the remnant.

G298.5-0.3: (Fig. 4) This object consists of a bright, narrow ridge of length 6' and possibly two other ridges lying parallel to the north-west. These are situated in a

complex of H II emission. Comparison with 60 μ m data shows that the brightest ridge is non-thermal, while the results are inconclusive for the other two ridges. If the main ridge alone is non-thermal, then the source may be extragalactic. If either of the other two ridges is also non-thermal, then the source is more likely a shell or composite SNR. Because of their similar orientation, it seems likely that the ridges are all associated and hence lie in our Galaxy. Higher resolution observations are required to aid interpretation of this object.

G298.6–0.0: (Fig. 5) An incomplete shell SNR. The MOST flux density of $S_{0.843} = 7.4$ Jy is much larger than that expected from the previous flux density estimates of $S_{0.408} = 5.6$ Jy (Shaver & Goss 1970; Green 1974) and $S_5 = 3.2$ Jy (Shaver & Goss 1970). However, the remnant lies in a complex region near two bright extended HII

regions, and previous measurements may have been affected by confusion.

G302.3+0.7: (Fig. 5) An SNR with evidence of a biannular structure in which a smaller (diameter $\sim 11'$) annulus in the south-east overlaps a larger (diameter $\sim 14'$) annulus in the north-west, both incomplete. The brightest emission occurs along the south-western and north-eastern borders, and a single, faint filament of length 10' lies outside the remnant in the south. Although confusion occurs because of the presence of a weak grating artifact in the region, the western end of the filament apparently intersects the remnant, while the eastern end projects towards a faint unresolved source lying several arcminutes away. Higher-sensitivity observations are required to determine if an association exists between the filament and the unresolved source, and also between the filament and the SNR. The filament resembles other non-thermal filaments found at the Galactic centre that are apparently associated with SNRs (e.g. Gray et al. 1991). The northern half of the remnant is partly confused with an HII region lying to the north-west.

G308.7+0.0: (Fig. 6) The source consists of a bright, elongated structure of extent $9' \times 3'$ (P.A. = 70°) lying within faint, diffuse nebulosity of dimensions $22' \times 7'$ elongated at a similar position angle. Using the Fleurs synthesis radio telescope at 1.415 GHz, Caswell et al. (1981) found evidence of shell-like structure in the brighter component, supported by the MOST contour map, although they note that if G308.7+0.0 is a shell SNR, then its appearance is peculiar because it does not have the characteristic sharply-defined outer perimeter. In addition, the emission is significantly more elongated than for a typical shell remnant. This structure suggests that G308.7+0.0 may instead be an example of a plerionic remnant with unusual morphology.

A faint but well-defined arc of length 15' lies 20' to the south-east at R.A. $(J2000) = 13^{h}43^{m}25^{s}$, Dec. $(J2000) = -62^{\circ}34'$. Caswell et al. (1992) suggest that this may be part of a large-diameter shell (G308.8-0.1), with G308.7+0.0 forming the north-western rim, which would then explain its elongation. There is widespread thermal radiation from much of this area, including the HII region in the north-eastern corner of the image, the bright compact source at R.A. $(J2000) = 13^{h}43^{m}1.8^{s}$, Dec. $(J2000) = -62^{\circ}08'56''$, and general diffuse thermal emission covering the field, making it difficult to decide what is non-thermal. The prominent bar on the western end of the arc appears to be thermal and therefore probably unrelated to the remnant. The non-thermal extension from the southern side of G308.7+0.0 contains a knot at R.A. $(J2000) = 13^{h}41^{m}42.3^{s}$, Dec. $(J2000) = -62^{\circ}20'12''$. This knot lies close to the young pulsar PSR J1341-6220 (Kaspi et al. 1992), although an association is still to be confirmed.

It is interesting to note that a striking resemblance exists between G308.7+0.0 and G320.4-1.2 (Fig. 12). Both remnants contain loosely-connected structures of which the north-western component more closely resembles plerionic structure than part of a shell. Furthermore, the southern extensions of the north-western components of both these SNRs also contain known pulsars.

G309.2–0.6: (Fig. 7) A complex SNR with a biannular structure consisting of multiple arcs of different curvature and an axis of symmetry at P.A.= 45°. The overall shape of the remnant suggests that 'blowouts' may have occurred in the north-east and south-west. The faint emission north of the remnant is thermal.

G309.8+0.0: (Fig. 7) Abundant thread-like emission exists within this shell, apparently extending outside the shell boundary in the west. A bright point source occurs at R.A. (J2000) = $13^{\rm h}50^{\rm m}35.2^{\rm s}$, Dec. (J2000) = $-62^{\circ}00'42''$, approximately 4' north of the geometric centre of the object, for which Caswell et al. (1980) find a possible optical counterpart lying within 2". They measure its 1.415 GHz flux density to be $S_{1.415} = 0.23$ Jy, while the MOST observations give $S_{0.843} = 0.39$ Jy, producing a spectral index of $\alpha_{0.843}^{1.415} = -1.0$. This is consistent with a background extragalactic source. The low Galactic latitude suggests that the optical identification may then be a chance stellar coincidence.

G310.6-0.3: (Fig. 8) This source has been the subject of some controversy. Previous observations (e.g. Milne 1969; Green 1974; Caswell & Clark 1975) were unable to separate the shell from the compact source lying 1' to the east. Both sources are found to be non-thermal in this work by comparing radio and 60 μ m IRAS data. However, the compact source is possibly extragalactic. Originally, Milne (1969) identified the shell source as an SNR. However, Caswell & Clark (1975) later concluded that the emission was probably thermal, based on a calculation of the flux density which indicated a reasonably flat spectral index. The present high-resolution observations, which are not as susceptible to confusion as the earlier observations, confirm the original indentification as an SNR. However, an accurate estimation of the spectral index awaits further observations at other frequencies.

G310.8–0.4: (Fig. 8) An SNR consisting of a bright arc in the east. The western half of the shell is seen only faintly and may be confused with diffuse thermal emission in the region. Comparison with 60 μ m IRAS images confirms that the bright arc is non-thermal. The structure lies in the same complex thermal region as G310.6–0.3, and there has been some debate about whether it is thermal or non-thermal. Milne (1969) originally dentified the source as an SNR. By contrast, Caswell & Clark (1975) concluded that it was probably thermal on the basis of its flat spectral index ($\alpha_{0.408}^5 = -0.20$) and the apparent

detection of hydrogen recombination line emission (Dickel & Milne 1972). However, the recombination lines were probably produced by the bright compact H II region which lies at the northern end of the arc and the abundant thermal filamentary emission to the west, both of which are confused with the arc in previous low-resolution ($\sim 3'$) observations.

G311.5-0.3: (Fig. 8) A small-diameter shell SNR. The resolution is not high enough to allow a detailed examination of the structure, but the MOST observations show for the first time that the object is a shell.

G312.4-0.4: (Fig. 9) An irregular SNR with an overall shell structure. The shell edge is sharp and well-defined in the north and east, but is more diffuse on other sides. The emission weakens towards the south of G312.4-0.4, giving the remnant a horseshoe appearance. A previously undetected faint arc, concave to the body of the remnant, lies 12' to the south, and there is evidence of a second filament of even fainter emission between this arc and the remnant. Variation in the density of the local ISM may account for the strong asymmetry in this remnant, with a cavity to the south of the pre-SN star perhaps necessary to explain the large distance of the southern arc from the remainder of the emission. Observations of G312.4-0.4 were made with the Parkes radiotelescope at 4.5 and 8.55 GHz in both total intensity and linearly polarised intensity (Whiteoak 1993b). Polarisation of up to 15% was detected at 8.55 GHz, while flux densities of $S_{4.5} = 30 \pm 2$ Jy and $S_{8.55} = 17 \pm 4$ Jy were measured. In conjunction with the flux densities determined by Caswell & Barnes (1985) of $S_{0.408} = 56$ Jy and $S_5 = 28$ Jy, a spectral index of $\alpha_{0.408}^{8.55} = -0.36 \pm 0.09$ is derived.

G315.4-0.3: (Fig. 9) A remnant with a puzzling structure. The image shows two bright small-diameter sources in the field, a faint narrow arc in the south-western corner of length $\sim 20'$, and several complex streamers of filamentary emission in the centre. The unresolved source at R.A. $(J2000) = 14^{h}37^{m}01.5^{s}$, Dec. $(J2000) = -60^{\circ}27'40''$ is non-thermal, has a steep spectral index, and may be extragalactic (Caswell et al. 1981). The MOST observations show that the small-diameter source (G315.31-0.27) situated within the extended emission at R.A. (J2000) = $14^{\rm h}35^{\rm m}06^{\rm s}$, Dec. (J2000) = $-60^{\circ}37'30''$ with $S_{0.843} = 0.87$ Jy has a close double structure. Previous work indicates that its spectral index is flat (Clark et al. 1975; Caswell et al. 1981), and it has hydrogen recombination line emission (Caswell & Haynes 1987). Comparison with IRAS data shows strong 60 μ m emission associated with this source, confirming that it is an HII region. The extended emission to the east and north of this HII region is nonthermal, although some faint thermal emission may also exist in the general area. The only well-defined, apparently non-thermal, shell component in the field is the arc in the south-western corner, and this seems to form a faint semi-circle around the HII region.

G315.4-2.3 (Fig. 10) A shell remnant with multiple arcs. The brightest emission comes from a ridge in the south-western corner which conspicuously protrudes outside the line of the main shell. The south-eastern side of the remnant appears to be composed of two arcs. Little emission is visible from the central part of the SNR, but the large angular size of this remnant means that a significant portion of its flux density will not be detected by the MOST. There is an interesting structure within the main shell on the western side which resembles yet another shell (diameter $\sim 12'$) centred at R.A. (J2000) = $14^{\rm h}41^{\rm m}00^{\rm s}$, Dec. $(J2000) = -62^{\circ}29'$. Optical emission from the nebula RCW 86 is associated with the remnant (Hill 1967; van den Bergh et al. 1973), forming a partial shell ($\sim 5'$ diameter) at the north-western end of the bright ridge of radio emission. An isolated optical filament (Hill 1967) is well-aligned with the northern part of the radio shell.

G315.9–0.0: (Fig. 10) A very low brightness shell. A peculiar feature is a straight, narrow jet-like structure extending radially outwards from the north-western side of the shell. Because the emission is very weak, the remnant has not yet been detected at other frequencies, and so the significance of the jet is unknown. Comparison of the MOST image with 60 μ m IRAS data confirms the nonthermal nature of the emission.

G318.9+0.4: (Fig. 11) A very peculiar composite SNR. The remnant consists of two components: a series of narrow, overlapping arcs, and a core feature offset to the east within the arc envelope (Whiteoak 1990, 1993a). The overall structure is highly elliptical, possessing an envelope that is more elongated than any other known Galactic shell remnant. The arcs are all unresolved in thickness in the MOST image, and form an unusual cusp at the southern end of the object. A north-south oriented ridge lies within the core component, and a faint jet-like structure extends from the eastern side of the core emission towards the adjacent arc.

G320.4–1.2: (Fig. 12) An unusual SNR consisting of two loosely connected emission regions that outline a shell. The brightest emission comes from the north-western component and consists of a roughly circular region (diameter 10') with a strong central peak. On closer inspection, the peak is found to be composed of four knots which form a ring of diameter 1'.3. The south-eastern component of G320.4–1.2 shows strong evidence of radially-oriented features in its emission. These interlocking arcs could be interpreted as a helical structure. A pulsar has been detected in G320.4–1.2 in both the X-ray (Seward & Harnden 1982) and radio (Manchester et al. 1982). It lies in the diffuse emission associated with the north-western radio component at R.A. (J2000) = $15^{\rm h}13^{\rm m}55.6^{\rm s}$,

Dec. (J2000) = $-59^{\circ}08'08''$ and is designated PSR J1513-5908 (Taylor et al. 1993). There is some uncertainty attached to the SNR/pulsar association, with several authors concluding that it is only a chance line-of-sight superposition of two unrelated phenomena (e.g. van den Bergh & Kamper 1984). There is no obvious radio counterpart to the X-ray nebula surrounding the pulsar (Seward et al. 1983, 1984; Seward 1990). X-ray emission also arises from the small ring in the north-western component, while optical emission overlaps this component from the $10' \times 8'$ H α nebula RCW 89.

G320.6–1.6: (Fig. 12) A large-diameter, filamentary remnant with multiple arcs and an incomplete shell structure. Two parallel arcs separated by 10' occur in the south, while the eastern emission consists of a series of filaments which taper to a single thread or jet in the north-east. The western side of this remnant overlaps the bright emission from the remnant G320.4–1.2. Comparison of the MOST image with 60 μ m IRAS data shows that G320.6–1.6 is non-thermal, consistent with the spectral index of $\alpha_{0.408}^5 = -0.47$ determined by Green (1974).

G321.9–0.3: (Fig. 13) An unusual feature of this shell SNR is a 3' extension from the southern rim that terminates in a knot of emission. Haynes (1987) observed this region with the MOST and found evidence of an association between G321.9–0.3 and Circinus X–1, the variable binary system 10' north of the remnant, whose associated radio emission is also shown in the image. He cites as evidence an alignment between the peak of Cir X–1, the line of its southern extension, the geometrical centre of G321.9–0.3, and the knot lying outside the shell of G321.9–0.3 to the south. However, IRAS data show significant 60 μ m emission from the southern knot which indicates a thermal source probably not associated with the remnant.

G322.5–0.1: (Fig. 13) A composite SNR consisting of a circular shell with an elliptical plerionic component lying close to the centre, and five knots located in the eastern half (Whiteoak 1992). The compact source at R.A. (J2000) = $15^{\rm h}23^{\rm m}42.6^{\rm s}$, Dec. (J2000) = $-57^{\circ}09'25''$ is the planetary nebula Pe 2-8 (Perek & Kahoutek 1967). Improved estimates for the flux densities are $S_{0.843} = 0.16 \pm 0.03$ Jy for the plerionic component and $S_{0.843} = 1.5 \pm 0.2$ Jy for the shell. Recent observations with the Parkes radio telescope at 4.5 GHz give a flux density of $S_{4.5} = 0.89 \pm 0.13$ Jy, implying an overall spectral index of $\alpha_{0.843}^{4.5} = -0.37 \pm 0.16$. Little evidence of polarised emission was found (Whiteoak 1993b).

G323.5+0.1: (Fig. 14) A faint shell remnant with a strangely rectangular shape. Comparison with 60 μ m data shows that the bright point source $\sim 2'$ west of the shell centre is thermal and therefore probably unrelated to the SNR.

G326.3-1.8: (Fig. 14) A composite SNR consisting of a filamentary shell and a bright plerionic component offset south-west of the centre. The whole shell is covered with abundant filamentary emission which is predominantly aligned in an east-west direction, coinciding with the direction of the magnetic field across the remnant (Milne et al. 1989). The remnant is too extended to allow a reliable flux density for the shell component to be determined from the MOST observations, but a good estimate can be made for the smaller plerionic component of $S_{0.843} =$ 22 Jy. The X-ray emission detected by Seward (1990) consists of a diffuse component covering the same area as the radio shell, and four discrete clumps that lie along a northeast/south-west diagonal passing close to the centre of the remnant. However, no X-ray clump is coincident with the radio plerionic component. Optical emission has also been detected, associated mainly with the northern and southern rims, but not the plerionic component (van den Bergh 1979; Zealey et al. 1979).

G327.1–1.1: (Fig. 15) A composite SNR with a faint shell and an unusual off-centre plerionic component which is composed of four knots forming a ring-like structure of diameter 3'. A peculiar feature is a 2' long ridge extending north-west from the western side of the plerionic component. The contribution of the plerionic component to the total flux density is 2.0 Jy. X-ray emission has been detected near the plerionic component (Seward 1990), but offset \sim 3' to the west (Lamb & Markert 1981). The small-diameter radio source outside the shell to the south-west in the image is thermal.

G327.4+0.4: (Fig. 15) A remnant possessing an unusual multi-ring structure. Milne et al. (1989) observed this SNR with the MOST, and described its structure as a series of shells emanating from the bright eastern rim. Lamb & Markert (1981) report the detection of X-ray emission which peaks near the remnant centre. The X-ray images of Seward (1990) show more detail, revealing faint patchy emission with a similar extent to the radio emission and interspersed with at least four bright concentrations. However, none of these concentrations appears to have a radio counterpart in the MOST image.

G332.4+0.1: (Fig. 17) An irregular shell SNR with a bright narrow rim. The eastern rim has a smaller curvature than the western rim, and could be interpreted as a second shell or blowout. Roger et al. (1985) and Kesteven et al. (1987) have presented MOST observations showing a jet and plume associated with the remnant, with the jet appearing as a faint, narrow extension emerging from the north-eastern side of the shell, and joining a plume which lies outside the image to the north-east. However, comparison with 60 μ m IRAS images shows that both the jet and plume are likely to be thermal and probably unrelated to the remnant. Indeed, Roger et al. (1985) find that

the jet has a flat spectral index ($\alpha_{0.843}^{8.4} = -0.05 \pm 0.1$) and no detectable polarisation, both consistent with a thermal origin. The plume has the same filamentary structure as the outlying emission of the nearby bright H II complex RCW 106 and is probably part of this emission.

G332.4—0.4: (Fig. 18) A much-studied shell remnant (e.g. Dickel et al. 1996). Bright optical filamentary emission has been detected from the associated nebula RCW 103 (van den Bergh et al. 1973). Optical arcs on the southern and north-western borders coincide with the regions of greatest radio brightness. X-ray observations (Nugent et al. 1984; Seward 1990) show that the remnant is also a strong source of X-ray emission. The *Einstein* Observatory HRI image of Seward (1990) shows a clear X-ray shell with a brightness distribution similar to the radio and optical. A compact X-ray source has been found very close to the shell centre which might be a hot neutron star (Tuohy & Garmire 1980), not detected in the MOST image above the central disk emission.

G335.2+0.1: (Fig. 18) A filamentary shell SNR. A prominent feature of the remnant is the striated emission within the shell. Comparison with 60 μ m IRAS maps suggest that the bright point source $\sim 4'$ west of the shell centre is non-thermal, but no further identification is possible at this stage.

G337.0-0.1: (Fig. 19) A peculiar non-thermal structure consisting of a circular plateau of faint emission in which several enhancements occur, and a bright ridge extending 4' north from the north-western edge of the plateau. The interpretation of this peculiar non-thermal object is uncertain and it is possible that part of it may be extragalactic. Much diffuse thermal emission in the region confuses the interpretation.

G337.2-0.7: (Fig. 20) The observations show for the first time a small-diameter circular shell remnant with maximum brightness along its southern boundary.

G337.3+1.0: (Fig. 20) A classic shell SNR. The shell is complete and almost circular, with several enhancements around the rim. Our flux density of $S_{0.843}=20$ Jy is somewhat larger than the previously published MOST value of 14.8 ± 3 Jy (Milne et al. 1989) and leads to a revised spectral index of $\alpha_{0.408}^{8.4}=-0.55$.

G337.8–0.1: (Fig. 21) A bright small-diameter SNR with a distorted shell. The MOST flux density of $S_{0.843} = 18$ Jy, combined with $S_{0.408} = 26$ Jy (Shaver & Goss 1970), gives a spectral index of $\alpha_{0.408}^{0.843} = -0.51$.

G338.1+0.4: (Fig. 21) The source consists of a faint semicircle describing the northern half of a shell, while the southern half cannot be separated from the general thermal emission in the region. Zealey et al. (1979) have de-

tected optical nebulosity coincident with the north-eastern radio emission.

G338.3-0.0: (Fig. 22) A broken shell SNR lying on the edge of the bright H II region G338.4+0.0 (part of the MSH 16-47 complex).

G338.5+0.1: (Fig. 22) A circular patch of faint non-thermal emission (diameter 5') lying on the northern edge of the bright H II region G338.4+0.0. The southern extent of the non-thermal emission is unclear, but the bright ridges and knots in the east and the south-west of the field are known to be thermal.

G340.4+0.4: (Fig. 23) A shell SNR with more internal structure than a simple annulus. The faint emission on the eastern and western sides of the bright central ringlike structure, not evident in previous observations of the remnant (e.g. Caswell et al. 1983a), results in elongation that may be due to a blowout.

G342.0-0.2: (Fig. 23) A shell SNR with internal structure. This object has a close companion remnant, G341.9-0.3, which Caswell et al. (1983a) suggest might be located at the same distance. The two remnants may be interacting.

G348.5–0.0 (Fig. 25) This object has recently been identified as a separate SNR in the CTB 37 complex by Kassim et al. (1991). The most prominent part of the remnant is a curved ridge which appears to be separated by $\sim 1'$ from the bright eastern rim of G348.5+0.1. At this stage it is not possible to say whether the two remnants are associated with the same region or are interacting in some manner.

G348.5+0.1: (Fig. 25) A confused region of nonthermal emission. The main structure is a shell, which has one of the highest mean surface brightnesses in this catalogue. Faint emission extends to the south-west, suggesting expansion into a cavity. Comparison with 60 μ m IRAS images shows that considerable diffuse thermal emission also exists in the region, perhaps accounting for some of the faint radio emission to the west.

G348.7+0.3: (Fig. 25) The MOST image shows a region of non-thermal emission that consists of a shell of diameter 7' and a faint plateau $\sim 13'$ in diameter which overlaps the south-eastern part of the shell. The plateau is approximately rectangular in shape and extends to the south as far as the remnant G348.5+0.1.

G351.2+0.1: (Fig. 26) An SNR with a distorted shell. High-resolution observations with the VLA by Becker & Helfand (1988) do not detect much of the extended emission evident here, but confirm the basic shell structure. They find a compact source with an inverted spectrum $(\alpha_{1.4}^{15} = +0.27)$ near the shell centre, which is too faint to

be seen in the MOST image. The association of this source with the shell has not been confirmed, and so we suggest a shell interpretation of the morphology rather than a composite at this stage. Becker & Helfand (1988) also detected a straight filament in the structure, but the MOST image shows this is simply part of the northern rim of the shell.

3.2. MSC.B Sources

G286.5–1.2: (Fig. 27) The main feature is a bright, curved filament 15' in length with a kink near its centre. A second, fainter filament lies north-west and almost parallel to the main filament. Although excluded from the MOST image, a bright non-thermal point source lies 30' to the north-west. Interestingly, both filaments are curved around this source, although an association between it and the filaments is unlikely because of their large angular separation. Another unresolved source at R.A. (J2000) $=10^{\rm h}34^{\rm m}14.4^{\rm s}$, Dec. (J2000) $=-59^{\circ}49'03''$ is non-thermal, while the slightly-extended source 5' to its north-west is an HII region. G286.5-1.2 resembles the Galactic nonthermal structure known as the "Snake" (Gray et al. 1991). The similarity between the Snake and the main filament in G286.5-1.2 is quite striking, with both structures having similar curvature and possessing a central kink.

G289.7–0.3: (Fig. 27) A very unusual shell SNR. It possesses a well-defined, roughly circular shell within which lies extensive, structured filamentary emission. The interior is dominated by two arcs of emission, together describing an elliptical shape. Two parallel filaments emerge radially from the south of this structure and extend to the southern part of the shell, joining it at the point where the shell emission is brightest. At least six other filaments are apparent in the western half of the remnant, producing a distinct cellular structure reminiscent of some planetary nebulae.

A barely-resolved source lies 1' north-east of the geometric centre of the shell. Observations of this source were made at 1.47 and 4.79 GHz with the ATCA (Whiteoak 1993b). Two small-diameter sources were found separated by 30", with spectral indices $\alpha_{1.47}^{4.79} = -1.2$ and -0.8 for the south-eastern and north-western components respectively. Their small angular separation and steepness of their spectral indices imply that they are part of the same extragalactic double source and therefore unrelated to G289.7–0.3.

While the morphology of G289.7–0.3 suggests it may be a shell SNR, a planetary nebula interpretation cannot be ruled out. In observations at 4.5 and 8.55 GHz with the Parkes radio telescope (Whiteoak 1993b), flux densities of $S_{4.5}=7.5\pm2.3$ Jy and $S_{8.55}=3.6\pm0.9$ Jy were determined respectively. With the MOST flux density of $S_{0.843}=6.4\pm0.5$ Jy, an overall spectral index of $\alpha_{0.843}^{8.55}=-0.2\pm0.2$ is obtained. There is a suggestion of a

turnover in the spectrum, implying that the emission may be thermal. The polarisation observations undertaken at Parkes indicate negligible polarisation at 4.5 GHz. Comparison between radio and IRAS 60 μ m data is inconclusive

Another possibility relates to the observation that Wolf-Rayet stars can produce rings of emission arising from heavy mass-loss either in their O star phase or through their own stellar winds and ejecta, coupled with strong ionising radiation (e.g. Marston et al. 1994). Offset to the north-west of the centre of G289.7-0.3 at R.A. $(J2000) = 11^{h}01^{m}02.3^{s}$, Dec. $(J2000) = -60^{\circ}14'01''$ lies the Wolf-Rayet star WR35b (Shara et al. 1991), a member of the open cluster Sher 1 (Moffat et al. 1991). It is possible that WR35b and other high-luminosity stars in Sher 1 have influenced the structure of G289.7-0.3, although the distance of 10 kpc (Moffat et al. 1991) implies a rather large shell size of ~ 50 pc. As an interesting note, fossil shells have also been detected around some Wolf-Rayet ring nebulae (Manchado et al. 1995). Although difficult to see here in the MOST image, a very faint shell of diameter $\sim 40'$ lies concentrically with G289.7–0.3, also apparent in the 5 GHz observations of Haynes, Caswell, & Simons (1978), that is reminiscent of such fossil shells. Clearly, further observations are required before the structure of G289.7-0.3 can be fully explained.

G294.1–0.0: (Fig. 28) A very faint large-diameter shell. Although the average surface brightness of 1.2 mJy/beam is barely above the noise, a well-defined rim characteristic of shell structure is apparent, with a pronounced bulge on its eastern side. Comparison with 60 μ m maps shows that the bright patch of emission adjoining the southern boundary is an H II region.

G299.6–**0.5**: (Fig. 28) A faint shell with brighter eastern rim. The small-diameter sources within the shell are all non-thermal.

G301.4–1.0: (Fig. 29) A faint, circular shell remnant possessing an unusual "blowout" on its south-western side. The blowout consists of a block of faint, striated emission extending 12′ in a south-westerly direction from a gap in the shell structure.

 $\mathbf{G308.1} - \mathbf{0.7:}$ (Fig. 29) A shell remnant with straight north-western edge.

G317.3-0.2: (Fig. 30) An object consisting of two opposing arcs. Some of the diffuse emission in the region may be associated with the nearby H II complex G316.8-0.1.

G318.2+0.1: (Fig. 30) A large-diameter shell SNR. This remnant is outlined by two non-thermal features that form the north-western and south-eastern sections of a shell. The north-western component consists of a single bright arc of length 30′, while the south-eastern

component is a band (dimensions $25' \times 17'$) composed of a number of curved, parallel filaments, similar to those of the blowout of G301.4–1.0. The faint north-western filament outside the shell at R.A. (J2000) = $14^{\rm h}52^{\rm m}08^{\rm s}$, Dec. (J2000) = $-58^{\circ}46'44''$ is non-thermal and may be related. The filamentary emission lying perpendicular to the northern boundary and centred at R.A. (J2000) = $14^{\rm h}55^{\rm m}38^{\rm s}$, Dec. (J2000) = $-58^{\circ}51'08''$ is also non-thermal. G318.2+0.1 was observed with the Parkes radio telescope in both total intensity and polarised intensity at 4.5 and 8.55 GHz (Whiteoak 1993b). The sensitivity was too low to provide accurate flux densities, but the non-thermal nature was confirmed by the polarisation observations which showed a polarisation of 10-20% at 4.5 GHz over the shell.

The central emission at R.A. (J2000) = $14^{\rm h}55^{\rm m}04^{\rm s}$, Dec. (J2000) = $-59^{\circ}02'44''$ is the H II region G318.223+0.140 (Haynes, Caswell, & Simons 1979). The bright clumps at R.A. (J2000) = $14^{\rm h}52^{\rm m}09^{\rm s}$, Dec. (J2000) = $-59^{\circ}10'07''$ and just to the south-east are also thermal.

G321.9–1.1: (Fig. 31) A faint shell remnant. Observed with the Parkes radio telescope at 4.5 GHz, the emission from the northern part of the shell appears to be polarised at a level of $\sim 15\%$ (Whiteoak 1993b), although this is uncertain because of the faintness of the radio emission.

G327.4+1.0: (Fig. 31) A faint, asymmetric shell, with bright western rim. The bright point-source to the south is confused with general thermal emission in the region, but is probably non-thermal.

G329.7+0.4: (Fig. 32) A large-diameter SNR candidate. The shell is quite diffuse compared to other SNRs, with few sharply-defined outer edges. Comparison with 60 μ m data shows only faint emission coincident with the shell structure, suggesting a non-thermal nature, but confusion with thermal emission in the region makes the identification as an SNR only tentative at this stage.

G342.1+0.9: (Fig. 32) A distorted shell. The bright point source to the south-east is non-thermal.

G343.1–0.7: (Fig. 33) An unusual remnant. The main shell is square-shaped (side 20'), and brightest along its southern boundary which consists of three bright sharp-edged arcs. A second shell of diameter 13' lies at the north-western corner of the main shell. Comparison with 60 μ m maps suggests that the main shell is non-thermal and the minor shell thermal.

G343.1-0.7 was observed with the Parkes radio telescope at 4.5 and 8.55 GHz in both total and polarised intensity (Whiteoak 1993b). The total intensity observations give flux densities of $S_{4.5}=3.9\pm0.6$ Jy and $S_{8.55}=2.4\pm0.5$ Jy for the main shell, and $S_{4.5}=4.0\pm0.3$ Jy and $S_{8.55}=2.6\pm0.6$ Jy for the smaller shell. The

MOST observations give flux densities of $S_{0.843} = 8.5 \pm 0.6$ Jy and $S_{0.843} = 4.5 \pm 0.3$ Jy for the main and minor shells respectively. Estimates of the corresponding spectral indices of the two components are then $\alpha_{0.843}^{8.55} = -0.55$ and -0.19. The main shell appears to be polarised at 4.5 GHz with levels up to about 12%, while no polarisation was detected from the minor shell. At 8.55 GHz, the main shell is found to be polarised to $\sim 20\%$, and again no polarised emission is associated with the minor shell. The main shell is clearly an SNR. The absence of polarised emission in the smaller shell, its flat spectral index, and the presence of 60 μ m emission indicates that the minor shell is probably thermal.

G345.7–0.2: (Fig. 33) A faint disk, with a peak just south of the centre lying close to the position of the pulsar PSR J1707-4053 (Taylor et al. 1993), although the large age of the pulsar ($> 10^6$ years) suggests a chance coincidence.

G349.2-0.1 (Fig. 34) A small-diameter shell with central emission lying on the edge of the HII region G349.1+0.0.

G351.7+0.8: (Fig. 34) A faint plateau of emission on the edge of a bright H II region. The pulsar PSR J1721–3532 is situated outside the eastern side of this structure at R.A. (J2000) = $17^{\rm h}21^{\rm m}32.8^{\rm s}$, Dec. (J2000) = $-35^{\circ}32'46.6''$ (Taylor et al. 1993), although it is obscured by a small H II region.

G351.9-0.9: (Fig. 35) A very faint shell-like object.

G354.8-0.8: (Fig. 35) A well-defined shell SNR with a complete boundary and rim enhancements along the eastern side and in the north-west.

3.3 Sources Reclassified

G299.0+0.2: (Fig. 36) The MOST image clarifies the nature of this region. The field contains several bright small-diameter sources and regions of faint extended emission. Comparison with 60 μ m IRAS data shows that all the extended emission in the region is thermal. The central compact source lying at R.A. (J2000) = $12^{\rm h}17^{\rm m}23.8^{\rm s}$, Dec. (J2000) = $-62^{\circ}29'01''$ is also thermal, as is the bright small-diameter source in the west. However, the bright unresolved source in the north-east of the field is non-thermal and possibly an unrelated background object. It is blending of this source and the extended thermal emission in the region that has previously simulated an SNR (e.g. Clark et al. 1975).

G328.0+0.3: (Fig. 36) Identified by Shaver & Goss (1970) as a region of extended non-thermal emission from low-resolution observations. However, the MOST image in conjunction with 60 μ m IRAS data shows that there

was confusion between a non-thermal unresolved source at R.A. $(J2000) = 15^h53^m19.4^s$, Dec. $(J2000) = -53^{\circ}27'54''$ which is probably extragalactic, and faint extended thermal emission in the region.

4. Discussion

Many questions remain unanswered concerning the distribution and evolution of SNRs. Two major difficulties still restricting progress are the lack of accurate distances for the vast majority of SNRs, and the small number of remnants known. The present work helps to alleviate the second problem, significantly increasing the number of known SNRs in the region surveyed. In addition, the higher resolution and sensitivity of the data allows the clarification of several hypotheses previously put forward, but based on more limited observations.

4.1. Completeness of sample

Fifty-seven previously-identified SNRs are located in the area covered by the MOST survey. More than half of these had not been observed at a resolution higher than $\sim 3'$. According to Green (1995), current catalogues are complete down to $\Sigma_{1\rm GHz}\sim 8~10^{-21} \rm Wm^{-2}Hz^{-1}sr^{-1}$ and angular size $\sim 8'$. These completeness limits are determined by the sensitivity of the observations and the resolution of the telescopes respectively. Figure 37 is a plot of surface brightness versus angular diameter for all known Galactic SNRs, with filled and hollow circles representing objects in Green's (1995) catalogue and the MSC catalogue respectively. The new MOST data make significant improvements over previous sensitivity limits and reveal many faint SNRs, but no small-diameter remnants and no new remnants with angular size $\geq 40'$. It is clear that the search is not uniformly sensitive over the whole region surveyed. Sensitivity is determined by a number of factors, one of which is the presence of confusing sources. As SNRs are found in greatly differing environments throughout the Galaxy, ranging from isolated locations to regions in close proximity to bright, complex sources, it is clear that the sensitivity will also vary.

There are 20 good candidates for SNRs newly identified from the MOST survey (i.e. MSC.B + two already in the literature and hence in MSC.A), increasing by more than 30% the number of remnants known. If, conservatively, half of MSC.C is also included, the increase is $\sim\!50\%$. To obtain a more precise estimate of the completeness of the MOST search, Figure 38 shows a histogram of surface brightness for all SNRs in Tables MSC.A and MSC.B. It is probable that the current list of southern SNRs is now complete down to a brightness $\sim 8\ 10^{-21}\ \rm Wm^{-2}Hz^{-1}sr^{-1}$.

The MOST is insensitive to smooth structure $\gtrsim 30'$, and so any SNR with smoothly-varying emission on this scale will be missed. However, sharp gradients in the sur-

face brightness of such objects will be detected and an SNR can be identified on this basis. On the smallest scale, the resolution of the MOST is such that shell structure will be apparent if its rim is bright and its diameter is >4'. Some of the small-diameter sources in MSC.C are probably extragalactic, as their morphologies are not typical of SNRs. It is unlikely that the careful search of the MOST records will have missed any shell with diameter $\gtrsim 4'$ to ~ 3 times the sensitivity limit of the observations. Identification of faint shells as non-thermal is more problematical. For faint, large-diameter remnants, it is more difficult to determine completeness. The MOST survey is known to contain much fine-scale structure extending over many degrees (Whiteoak et al. 1994), and although comparison with 60 μ m IRAS data indicates that most of this radio emission is thermal, further work is needed to determine whether or not a non-thermal component is present, possibly indicating very large remnants.

4.2. Distribution in the Galaxy

One of the areas in the investigation of SNRs that continues to be a source of much discussion concerns their distances. HI absorption line measurements are thought to give fairly accurate estimates, but have been made for only a few of the brightest objects (e.g. Caswell et al. 1975). None of the new identifications in this paper would be bright enough to attempt such measurements. Historically, distances have been estimated using Σ -D diagrams, calibrating the scale with the few SNRs that are known to have reliable distances. However, it has been shown that for a particular surface brightness, individual diameters can vary by up to a factor of ten, negating the usefulness of this method (Green 1991). It is not known whether this scatter is a result of intrinsic differences in SNR formation or variation in the local environment.

Despite the lack of distance information, it is possible to draw some conclusions by considering the distribution of SNR brightness against various parameters. Figure 39 shows the distribution of surface brightness with Galactic longitude. Remnants in the MOST survey are shown as hollow circles, while the filled circles are from Green (1995). No new SNRs were detected between $l = 245^{\circ}$ and 286°. In the anticentre direction (90° $\leq l \leq 270^{\circ}$), almost all the SNRs will be relatively close and the proportion visible in the narrow strip of the survey ($|b| \leq 1.5^{\circ}$) will be small. As previously noted by Green (1995), most of the known SNRs in the anticentre region are faint. It is not possible to determine from this work whether this reflects the greater confusion in more complex regions closer to the Galactic centre, or is indicative of a real difference in the remnant formation, perhaps occurring as a result of the lower ISM density in the anticentre. However, Fig. 39 does show that the southern part of the Galaxy is now better searched and more closely resembles the northern To give an idea of how extensive this survey has been, studies of other spiral galaxies have shown that SN populations are tightly clustered around their respective galactic equators with a scale height of $\sim\!100$ pc (Blaauw 1985). It seems probable that this kind of distribution also applies to our Galaxy and hence, although the MOST survey represents only a narrow wedge through the southern Milky Way, it in fact covers $\sim\!90\%$ of the volume expected to be populated there by SNRs.

4.3. Morphology

The morphologies of the vast majority of the SNRs observed in this work have now been determined with confidence. Of the 75 sources listed in MSC.A and MSC.B, only two (G298.5-0.3 and G315.4-0.3) have been difficult to classify. Several others have basic shell or composite structures, but details remain unclear. As a result of uncertainty in the identifications of MSC.C, only MSC.A and MSC.B sources are considered in this section. An interesting point to note is that no pure plerions were discovered. This is unexpected because $\sim 10\%$ of SNRs in Green's (1995) catalogue are plerions, and results primarily from the fact that the observations presented here have significantly higher resolution and sensitivity than previous data, allowing shell structure to be resolved in many cases. It should also be noted that SNR type is assigned by visual inspection. A total of 85% of the SNRs imaged have a simple shell structure, 12\% exhibit a composite morphology and 3% are unclear.

Few of the remnants possess the single circular shell brightness distribution expected for a 'classic' remnant (e.g. van der Laan 19692a, b). Several theories exist which attempt to explain the multiple arcs observed in almost a third of the SNRs in this work. Manchester (1987) suggests that a biconical flow has occurred at some stage in the SNR evolution, perhaps even prior to the SN explosion, which forms a biannular structure after interacting with the shock and ejecta from the SNR explosion. Kesteven & Caswell (1987) propose that such a structure could result from an inherently barrel-shaped SNR, with the various remnant shapes arising from different viewing perspectives. The MOST images show such great variation in their multi-shell structure that it is difficult to fit all SNRs into these simple models. It may eventuate that SNR structure simply reflects a non-uniform density in the surrounding ISM.

4.4. Orientation

Lack of circular symmetry is a commonly observed characteristic of SNR shells. It has been suggested by Roger et al. (1988) that the motion of the SN shock front and ejecta relative to the direction of the local Galactic magnetic field could produce elongation and planes of symmetry that lie parallel to the field lines, a possibility also considered by

Caswell (1979) who studied the effect of the magnetic field on the structure of plerions. The average increase of the density of the ISM nearer the Galactic plane could also potentially result in enhancement of emission from that half of a shell that lies at lower Galactic latitude (Caswell 1977; Shaver 1982). The present catalogue allows these effects to be further investigated, as it represents a uniform sample of southern SNRs close to the Galactic plane, and avoids some of the earlier problems such as low resolution and a small number of objects.

It was found that the angle of the major axis with respect to the Galactic plane had a random distribution for both shell elongation and plerion elongation. This suggests that any effect on the evolution by the large-scale Galactic magnetic field (known to be approximately parallel to the plane at low latitudes) is being dominated by more local influences. The question of preferential enhancement of the side of an SNR closer to the Galactic plane was studied by splitting each SNR shell into halves nearer and further from the plane. The flux densities of the two halves were considered separately, then normalised, and summed. Account was taken of the warp in the Galactic plane which causes the ridge of maximum gas density to lie somewhat south of zero Galactic latitude over much of the survey region. No statistical difference in flux density was found between the two halves, once again implying that local influences are more important in determining the brightness distribution of an SNR. Further investigation of the possible interaction of remnants with the surrounding ISM or neighbouring HII complexes will only be feasible when better distance estimates are available.

4.5. Size

Much of the analysis concerning the size of SNRs is severely limited by the lack of accurate distance information. It would be valuable to use the new data to investigate the distribution of linear size as a function of distance (Z) above the Galactic plane, for comparison with earlier findings that linear diameters (for an SNR of a given age) are larger at higher Z because of the lower average ISM density (Caswell & Lerche 1979). Taking those SNRs in the catalogue for which reliable distances are known, ranging in Z from 0 to 73 pc, there appears to be little dependence of diameter on Z. However, a thorough analysis of such a trend requires that SNR age also be taken into account.

Some conclusions can be drawn by considering the angular diameter as a function of Galactic longitude (Fig. 40), without the uncertainties involved in converting to linear diameters. It is probable that most of the SNRs in the anticentre hemisphere ($90^{\circ} \leq l \leq 270^{\circ}$) will be locally distributed, and will consequently tend to have larger than average angular diameters. This is in fact evident in Fig. 40.

When the region closer to the Galactic centre is searched, a lack of small-diameter remnants is also apparent (Green 1989; Helfand & Chanan 1989). A possible explanation for the observed deficit of small-diameter SNRs is that the progenitor star creates a bubble of low density gas via stellar winds prior to the explosion. As the SNR evolves in the free-expansion phase, little emission is generated until the shock impinges on the surface of the bubble and the surrounding ISM (Berkhuijsen 1986; Srinivasan & Bhattacharya 1988). Studies have shown that bubbles of hot, low-density gas with radii ~ 30 pc regularly occur for OB stars (Castor et al. 1975; Srinivasan & Bhattacharya 1988). The observed deficiency of small-diameter remnants is then likely to be a result of such an evolutionary path which would generate a larger object of detectable brightness in a relatively short period. Indeed, taking a conservative estimate of 15 pc radius on average for the low-density shell around an OB star would lead to a deficit of SNR shells in our Galaxy below a diameter of $\sim 5'$, fully consistent with the lower cutoff suggested in Fig. 40.

The situation with large-diameter SNRs is also anomalous. It is surprising that no new candidates were found with angular diameters > 40'. Smooth structure on this scale would not be detected by the MOST, but steep gradients in the shell would be apparent. Indeed, the shell of the Vela remnant, with a diameter of 7°, is clearly visible in the MOST data. An explanation for this phenomenon might lie in the fact that the MOST survey shows an abundance of large-scale faint emission along the plane (Whiteoak et al. 1994), much of which cannot conclusively be identified as either thermal or non-thermal at this stage. It is possible that some of this structure represents emission from the large shells of old remnants which will be apparent only when the MOST has completed a survey of a much larger area of the sky.

5. Conclusion

The MSC catalogue presents greyscale images and contour maps of all known SNRs lying within 1.5° of the southern galactic plane, complete down to $\sim 8 \cdot 10^{-21}$ $\mathrm{Wm^{-2}Hz^{-1}sr^{-1}}$. Many of the SNRs have been imaged at a substantially higher resolution and sensitivity than previously, allowing their detailed structure to be studied for the first time. Eighteen newly-discovered remnants were also presented, and another sixteen have been listed as candidates. The vast majority of the remnants in the catalogue were found to possess a shell structure. However, very few of these exhibited the 'classic' shell brightness distribution, with almost a third displaying a multiple shell structure. Various hypotheses concerning the interaction between the SNRs and the large-scale properties of the Galaxy were discussed, and it was found that the local ISM plays the dominant role in determining the brightness distribution of an SNR.

Acknowledgements. The authors wish to thank Lawrence Cram for his helpful comments concerning this paper. The MOST is operated with funds from the Australian Research Council and the Science Foundation for Physics within the University of Sydney.

References

Becker R.H., Helfand D.J., 1988, AJ 95, 883

Berkhuijsen E.M., 1986, A&A 166, 257

Blaauw A., 1985, in: Boland B.C., van Woerden H. (eds.) Astrophys. & Sp. Sc., No. 120, Birth and Evolution of Massive Stars and Stellar Groups. D. Reidel, Dordrecht, p. 211

Broadbent A., Haslam C.G.T., Osborne J.L., 1989, MNRAS 237, 381

Bignami G.F., Caraveo P.A., Goldwurm A., Mereghetti S., Palumbo G.G.C., 1986, ApJ 302, 606

Caswell J.L., Lerch I., 1979, MNRAS 187, 201

Castor J., McCray R., Weaver R., 1975, ApJ 200, L107

Caswell J.L., Barnes P.J., 1983, ApJ 271, L55

Caswell J.L., Barnes P.J., 1985, MNRAS 216, 753

Caswell J.L., Clark D.H., 1975, Aust. J. Phys. Astrophys. Suppl. 37, 57

Caswell J.L., Haynes R.F., 1987, A&A 171, 261

Caswell J.L., Milne D.K., Wellington K.J., 1981, MNRAS 195, 89

Caswell J.L., Murray J.D., Roger R.S., Cole D.J., Cooke D.J., 1975, A&A 45, 239

Caswell J.L., Haynes R.F., Milne D.K., Wellington K.J., 1980, MNRAS 190, 881

Caswell J.L., Haynes R.F., Milne D.K., Wellington K.J., 1983a, MNRAS 203, 595

Caswell J.L., Haynes R.F., Milne D.K., Wellington K.J., 1983b, MNRAS 204, 915

Caswell J.L., Haynes R.F., Milne D.K., Wellington K.J., Smith R.M., 1983c, Proc. Astron. Soc. Aust. 5, 227

Caswell J.L., Kesteven M.J., Stewart R.T., Milne D.K., Haynes R.F., 1992, ApJ 399, L151

Clark D.H., Caswell J.L., Green A.J., 1975, Aust. J. Phys. Astrophys. Suppl. 37, 1

Dickel J.R., Milne D.K., 1972, Aust. J. Phys. 25, 539

Dickel J.R., Green A.J., Ye T., Milne D.K., 1996, AJ 111, 340Elliott K.H., Malin D.F., 1979, MNRAS 186, 45

Gray A.D., Cram L.E., Ekers R.D., Goss W.M., 1991, Nat 353, 237

Green A.J., 1974, A&AS 18, 267

Green D.A., 1989, AJ 98, 1358

Green D.A., 1991, PASP 103, 209

Green D.A., 1995, in: McRay R., Wang Z. (eds.) Supernovae and Supernova Remnants. Cambridge Uni. Press, (in press) Haynes R.F., 1987, Aust. J. Phys. 40, 741

Haynes R.F., Caswell J.L., Simons L.W.J., 1978, Aust. J. Phys. Astrophys. Suppl. 45, 1

Haynes R.F., Caswell J.L., Simons L.W.J., 1979, Aust. J. Phys. Astrophys. Suppl. 48, 1

Helfand D.J., Chanan G.A., 1989, AJ 98, 1652

Hill E.R., 1967, Aust. J. Phys. 20, 297

Hutchings J.B., Crampton D., Cowley A.P., 1981, AJ 86, 871
Kaspi V.M., Manchester R.N., Johnston S., Lyne A.G., D'Amico N., 1992, ApJ 399, L155

Kassim N.E., Baum S.A., Weiler K.W., 1991, ApJ 374, 212

Kesteven M.J., Caswell J.L., 1987, A&A 183, 118

Kesteven M.J., Caswell J.L., Roger R.S., Milne D.K., Haynes R.F., Wellington K.J., 1987, Aust. J. Phys. 40, 855

Lamb R.C., Markert T.H., 1981, ApJ 244, 94

Longmore A.J., Clark D.H., Murdin P., 1977, MNRAS 181, 541

Manchado A., Garcia-Segura G., Chu Y.-H., 1995, in: van der
Hucht K.A., & Williams P.M. (eds.), IAU Symp. No. 163,
Wolf-Rayet Stars: Binaries, Colliding Winds, Evolution.
Kluwer, Dordrecht, p. 74

Manchester R.N., 1987, A&A 171, 205

Manchester R.N., Durdin J.M., 1983, in: Danziger J., & Gorenstein P. (eds.), IAU Symp. No. 101, Supernova Remnants and their X-ray Emission. Reidel, Dordrecht, p. 421

Manchester R.N., Tuohy I.R., D'Amico N., 1982, ApJ 262, L31 Markert T.H., Lamb R.C., Hartman R.C., Thompson D.J., Bignami G.F., 1981, ApJ 248, L17

Marston A.P., Yocum D.R., Garcia-Segura G., Chu Y.-H., 1994, ApJS 95, 151

Mills B.Y., 1981, Proc. Astron. Soc. Aust. 4, 156

Milne D.K., 1969, Aust. J. Phys. 22, 613

Milne D.K., Caswell J.L., Haynes R.F., Kesteven M.J., Wellington K.J., Roger R.S., Bunton J.D., 1985, Proc. Astron. Soc. Aust. 6, 78

Milne D.K., Caswell J.L., Kesteven M.J., Haynes R.F., Roger R.S., 1988, in: Kundt W. (ed.) Supernova Shells and their Birth Events. Springer-Verlag, p. 98

Milne D.K., Caswell J.L., Kesteven M.J., Haynes R.F., Roger R.S., 1989, Proc. Astron. Soc. Aust. 8, 187

Moffat A.F.J., Shara M.M., Potter M., 1991, AJ 102, 642

Nugent J.J., Becker R.H., Garmire G.P., Pravdo S.H., Tuohy I.R., Winkler P.F. Jr., 1984, ApJ 284, 612

Perek L., Kahoutek L., 1967, in: Catalogue of Galactic Planetary Nebulae. Academia Pub. House, Prague, p. 104

Robertson J.G., 1991, Aust. J. Phys. 44, 729

Roger R.S. Milne D.K., Caswell J.L., Little A.G., 1986, MNRAS 219, 815 Roger R.S., Milne D.K., Kesteven M.J., Haynes R.F., Wellington K.J., 1985, Nat 316, 44

Roger R.S., Milne D.K., Kesteven M.J., Wellington K.J., Haynes R.F., 1988, ApJ 332, 940

Seward F.D., 1990, ApJS 73, 781

Seward F.D., Harnden F.R., 1982, ApJ 256, L45

Seward F.D., Clark D.H., Harnden F.R., Murdin P.G., 1983, ApJ 267, 698

Seward F.D., Harnden F.R., Szymkowiak A., Swank J., 1984, ApJ 281, 650

Shara M.M., Moffat A.F.J., Smith L.F., Potter M., 1991, AJ 102, 716

Shaver P.S., Goss W.M., 1970, Aust. J. Phys. Astrophys. Suppl. 14, 133

Shaver P.S., 1982, A&A 105, 306

Srinivasan G., Bhattacharya D., 1988, in: Kundt, W. (ed.) Supernova Shells and their Birth Events. Springer-Verlag, Berlin, p. 15

Taylor J.H., Manchester R.N., Lyne A.G., 1993, ApJS 88, 529Tuohy I.R., Garmire G.P., 1980, ApJ 239, L107

van den Bergh S., 1979, ApJ 227, 497

van den Bergh S., Kamper K.W., 1984, ApJ 280, L51

van den Bergh S., Marscher A.P., Terzian Y., 1973, ApJS 26, 19

van der Laan H., 1962a, MNRAS 124, 125

van der Laan H., 1962b, MNRAS 124, 179

Whiteoak J.B.Z., 1990, Nat 347, 157

Whiteoak J.B.Z., 1992, MNRAS 256, 121

Whiteoak J.B.Z., 1993a, ApJ 415, 701

Whiteoak J.B.Z., 1993b, Ph.D. Thesis, University of Sydney

Whiteoak J.B.Z., Large M. I., Cram L. E., Piestrzynski B., 1989, Proc. Astron. Soc. Aust. 8, 176

Whiteoak J.B.Z., Cram L.E., Large M.I., 1994, MNRAS 269, 294

Wilson A.S., 1986, ApJ 302, 718

Woermann B., Jonas J.L., 1988, MNRAS 234, 971

Zealey W.J., Elliott K.H., Malin D.F., 1979, A&AS 38, 39



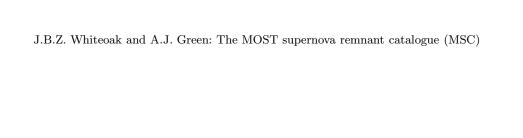
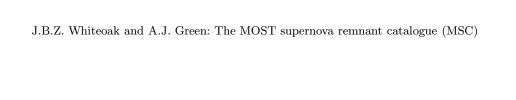


Fig. 2. (Upper) Contour map and greyscale image of G290.1-0.8; (Lower) Contour map and greyscale image of G291.0-0.1

346	J.B.Z. Whiteoak and A.J. Green: The MOST supernova remnant catalogue (MSC)
Fig. 3. (Upper) Cont	our map and greyscale image of G293.8 \pm 0.6; (Lower) Contour map and greyscale image of G296.1 \pm 0.5



 $\textbf{Fig. 4.} \ (\textit{Upper}) \ \text{Contour map and greyscale image of G296.8} - 0.3; \ (\textit{Lower}) \ \text{Contour map and greyscale image of G298.5} - 0.3$

348	J.B.Z. Whiteoak and A.J. Green: The MOST supernova remnant catalogue (MSC)
Fig. 5. (Upper) Conto	our map and greyscale image of G298.6-0.0; (Lower) Contour map and greyscale image of G302.3+0.7

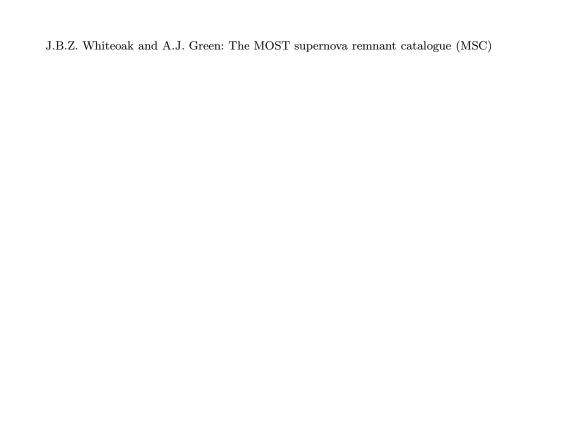


Fig. 6. (Upper) Contour map and greyscale image of G304.6+0.1; (Lower) Contour map and greyscale image of G308.7+0.0



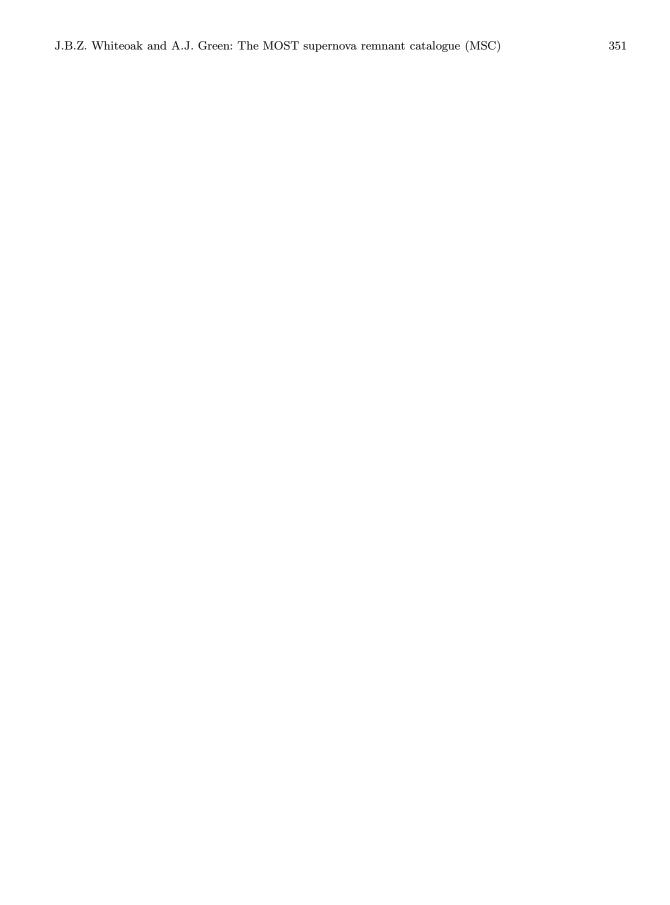


Fig. 8. (Upper) Contour map and greyscale image of G310.6-0.3 and G310.8-0.4; (Lower) Contour map and greyscale image of G311.5-0.3

352	J.B.Z. Whiteoak and A.J. Green: The MOST supernova remnant catalogue (MSC)
Fig. 9. (Upper) Conte	our map and greyscale image of G312.4 -0.4 ; (Lower) Contour map and greyscale image of G315.4 -0.3

354	J.B.Z. Whiteoak and A.J. Green: The MOST supernova remnant catalogue (MSC)
Fig. 11. (<i>Upper</i>) Con	tour map and greyscale image of G316.3 -0.0 ; (Lower) Contour map and greyscale image of G318.9 $+0.4$

356	J.B.Z. Whiteoak and A.J. Green: The MOST supernova remnant catalogue (MSC)
Fig. 13. (<i>Upper</i>) Cont	sour map and greyscale image of G321.9-0.3; (Lower) Contour map and greyscale image of G322.5-0.1



358	J.B.Z. Whiteoak and A.J. Green: The MOST supernova remnant catalogue (MSC)	
Fig. 15. (<i>Upper</i>) Cont	tour map and greyscale image of G327.1-1.1; (Lower) Contour map and greyscale image of G327.4+0.	4

360	J.B.Z. Whiteoak and A.J. Green: The MOST supernova remnant catalogue (MSC)
Fig. 17. (<i>Upper</i>) Conf	tour map and greyscale image of G332.0+0.2; (Lower) Contour map and greyscale image of G332.4+0.1
J (11)	

Fig. 18. (Upper) Contour map and greyscale image of G332.4-0.4; (Lower) Contour map and greyscale image of G335.2+0.1

362	J.B.Z. Whiteoak and A.J. Green: The MOST supernova remnant catalogue (MSC)
Fig. 19. (<i>Upper</i>) Con	tour map and greyscale image of G336.7+0.5; (Lower) Contour map and greyscale image of G337.0-0.1

364	J.B.Z. Whiteoak and A.J. Green: The MOST supernova remnant catalogue (MSC)
Fig. 21. (<i>Upper</i>) Con	tour map and greyscale image of G337.8-0.1; (Lower) Contour map and greyscale image of G338.1+0.4

366	J.B.Z. Whiteoak and A.J. Green: The MOST supernova remnant catalogue (MSC)	
Fig. 23. (<i>Upper</i>) Cont of G341.9–0.3 and G3	tour map and greyscale image of G340.4+0.4 and G340.6+0.3; ($Lower$) Contour map and greyscale im $342.0-0.2$	age

F of

368	J.B.Z. Whiteoak and A.J. Green: The MOST supernova remnant catalogue (MSC)	
Fig. 25. (Upper) Congreyscale image of G34	tour map and greyscale image of G348.5+0.1, G348.5-0.0, and G348.7+0.3; (Lower) Contour map and $49.7+0.2$	

F gr

370	J.B.Z. Whiteoak and A.J. Green: The MOST supernova remnant catalogue (MSC)
Fig. 27. (<i>Upper</i>) Cont	tour map and greyscale image of G286.5–1.2; (Lower) Contour map and greyscale image of G289.7–0.3

372	J.B.Z. Whiteoak and A.J. Green: The MOST supernova remnant catalogue (MSC)
Fig. 29. (Unner) Cont	tour map and greyscale image of G301.4-1.0; (Lower) Contour map and greyscale image of G308.1-0.7
- 18. 20. (Opper) Cont	war map and gregorate image of Goot. 1 1.0, (2000) Comour map and gregorate image of Goot.1-0.7

374	J.B.Z. Whiteoak and A.J. Green: The MOST supernova remnant catalogue (MSC)
Fig. 31. (<i>Upper</i>) Conf	tour map and greyscale image of G321.9-1.1; (Lower) Contour map and greyscale image of G327.4+1.0
G (-1F) 30m	

Fig. 32. (Upper) Contour map and greyscale image of G329.7+0.4; (Lower) Contour map and greyscale image of G342.1+0.9

376	J.B.Z. Whiteoak and A.J. Green: The MOST supernova remnant catalogue (MSC)
Fig. 33. (<i>Upper</i>) Con	tour map and greyscale image of $G343.1-0.7$; (Lower) Contour map and greyscale image of $G345.7-0.2$



378	J.B.Z. Whiteoak and A.J. Green: The MOST supernova remnant catalogue (MSC)
D. 07 (T.) 7	
Fig. 35. (<i>Upper</i>) Con-	tour map and greyscale image of G351.9-0.9; (Lower) Contour map and greyscale image of G354.8-0.3

	Fig. 39. Surface brightness versus longitude for known Galactic SNRs. Symbols as in Fig. 27
	tic SNRs. Symbols as in Fig. 37
Fig. 37. Surface brightness versus angular diameter for known SNRs. Hollow circles represent SNRs from this paper (MSC.A and MSC.B), while filled circles represent other known Galactic remnants	
Fig. 38. Histogram showing the number of remnants versus surface brightness	$ \begin{tabular}{ll} \bf Fig.~40.~Angular~diameter~versus~longitude~for~known~Galactic~SNRs.~Symbols~as~in~Fig.~37 \end{tabular} $

 ${\rm J.B.Z.}$ Whiteoak and ${\rm A.J.}$ Green: The MOST supernova remnant catalogue (MSC)